Experimental simulation of active control with on-line system identification on sound transmission through an elastic plate

An adaptive control algorithm with on-line system identification capability has been developed . One of the great advantages of this scheme is that an additional system identification mechanism such as an additional uncorrelated random signal generator as the source of system identification [Eriksson and Allie, J. Acoust. Soc. Am. 85, 797-802 (1989)] is not required. A time-varying plate-cavity system is used to demonstrate the control performance of this algorithm. The time-varying system consists of a stainless-steel plate which is bolted down on a rigid cavity opening where the cavity depth was changed with respect to time. For a given externally located harmonic sound excitation, the system identification and the control are simultaneously executed to minimize the transmitted sound in the cavity. The control performance of the algorithm is examined for two cases. First, all the water was drained, the external disturbance frequency is swept with 1 Hz/sec. The result shows an excellent frequency tracking capability with cavity internal sound suppression of 40 dB. For the second case, the water level is initially empty and then raised to 3/20 full in 60 seconds while the external sound excitation is fixed with a frequency. Hence, the cavity resonant frequency decreases and passes the external sound excitation frequency. The algorithm shows 40 dB transmitted noise suppression without compromising the system identification tracking capability.

INTRODUCTION

Noise suppression within the payload compartment of launch vehicles is one of the proposed applications of ANC technology. Turbulence generated by solid rocket motor plume at liftoff stage, and shockwave and turbulent boundary layer and their interaction in the ascent phase define the external acoustic environment. The structural vibrations caused by the external environment can create sound-pressure levels as high as 130 dB within the compartment. These acoustic loads impinge on increasingly delicate and complex payloads and some times results in payloads failure.

In order to alleviate this problem, acoustic blankets are used on the inside of the payload fairings for most launch vehicles. These 1- to 2-inch thick fiberglass blankets work well for high-frequency noise (above 400 Hz), but, like most passive sound suppression techniques their performance deteriorates at lower frequencies. The use of viscoelastic materials to suppress the noise within payload fairings has also been considered. This technique – as we will discuss – will not be effective on all the modes within the fairing.

ANC has the potential to suppress noise over a wide frequency band – especially low frequencies; it has the additional advantage of being lighter than passive methods. However, the launch vehicle environment poses some challenges that will require further research before an effective system can be realized. A typical launch vehicle is in the atmospheric region for approximately 60 s during its ascent; after this time, acoustics is obviously not an issue. An adaptive control algorithm for launch vehicles will therefore have to suppress payload compartment noise to an acceptable level (converge) in a few seconds, while monitoring any changes in the system for at least 1 minute. Therefore, one of these challenges is the need for an adaptive control algorithm that can adequately identify the time-dependent characteristics of the components in launch vehicles.

Our new efficient rapid convergent algorithm with on-line system identification capability will be described. The algorithm will be tested for its control performance using the time-varying plate-cavity system. The experimental simulation setup for the time-varying plate cavity system, which simulates a launch vehicle payload compartment, will be described in Sec. 1. The development of our efficient rapid convergent algorithm with on-line system identification will be discussed in Sec. II. Results of experiments to demonstrate the control performance of control algorithms will be presented in Sec. III.

I. Experimental Simulation Setup

A. Description of the model

The setup used in this simulation is shown in Fig. 1. It consists of a rectangular cavity (of width a, length b, and depth d) with the top wall at $z = 0$ being a rectangular flexible plate and the bottom wall at $z = -d$. The plate is simply supported and imbedded in an infinite rigid baffle in the $z = 0$ plane. The dimensions of the cavity used in this study are $a = 329$ mm, $b = 481.4$ mm and $d = 829.47$ mm (see Figure 1). Other parameters are: plate thickness $h_p = 0.9144$ mm, plate density $P_p = 8.5 \times 10^3$ kg/m^3, plate Young's modulus $E_p = 10.4 \times 10^{10}$ N/m^2, Poisson ratio $\nu = 0.3$, and speed of sound $c = 344$ m/s for the semi-infinite space ($z > 0$), and variable sound speed due to the cavity temperature change inside the cavity. An external sound source, located at a point x_0 excites the plate. The plate, in turn radiates sound into the cavity. The piezoelectric actuators are bounded symmetrically (on top and bottom of the plate as shown in Fig. 1). They are used to control the vibrational response of the plate to minimize sound transmission through the plate into the cavity.

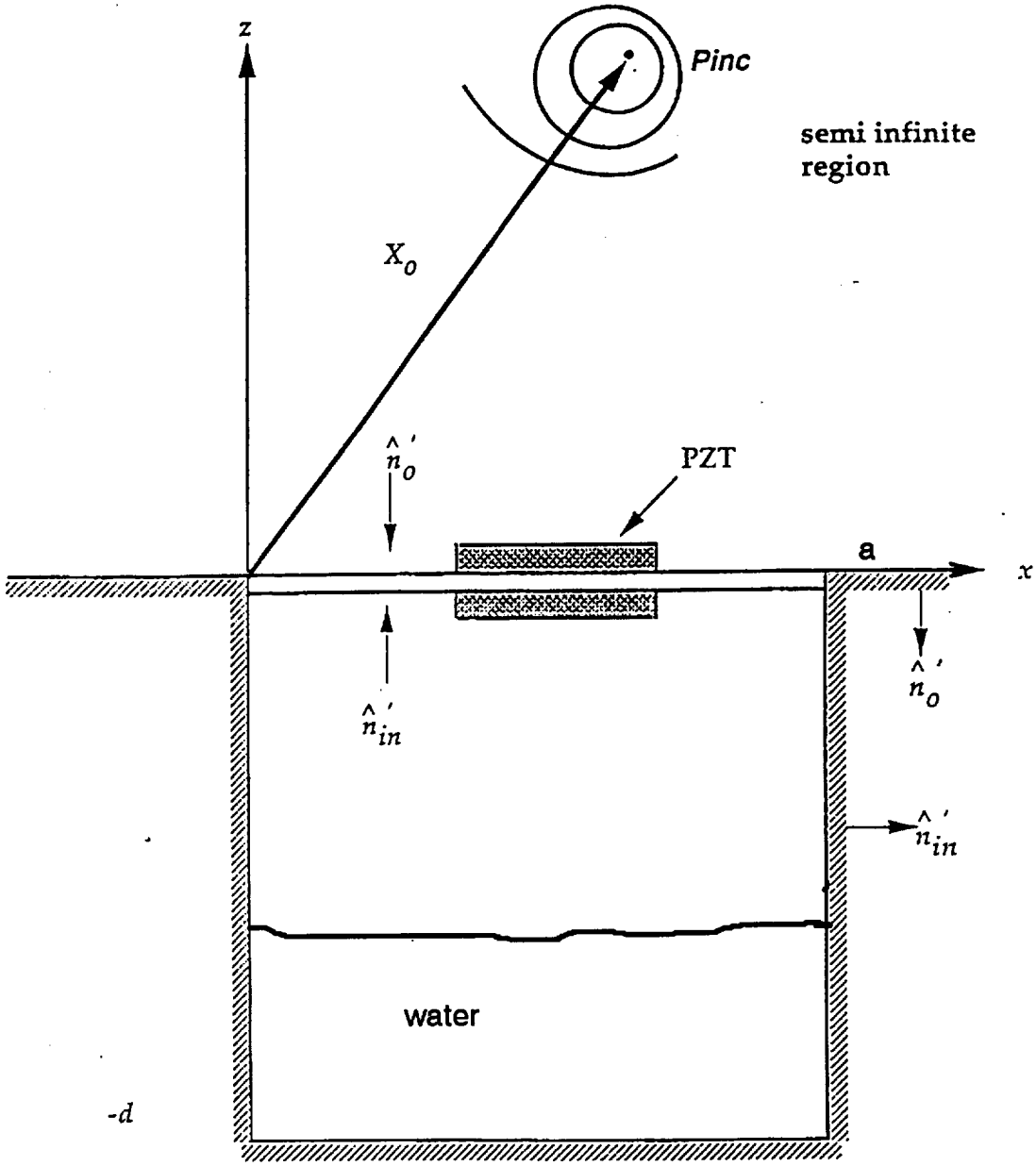
z
Pinc
semi infinite region
X_o
$\hat{n}_o'$
PZT
a
x
$\hat{n}_{in}'$
$\hat{n}_o'$
$\hat{n}_{in}'$
water
-d

FIGURE 1

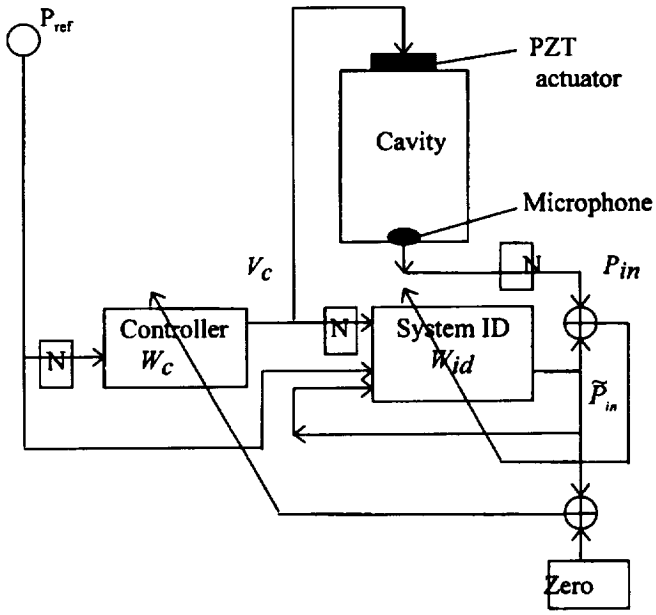

Fig. 2, Block diagram of experimental setup

II CONTROL ALGORITHMS

In this section, the algorithm for an adaptive controller with on-line system identification will be developed.

Figure 2 shows the block diagram of the simulation setup, where *N* in the figure signifies a normalization. The *k*th time step reference pressure $p_{ref}(k)$ is calculated using Eq. (2) at $x = -0.01$ m, $y = 0.1$ m, and $z = 1$ m and is fed to the controller and the system identification. The control voltage $V_c(k)$ is generated from the controller and is expressed as

$$V_c(k) = \sum_{i=0}^{N_c} W_c(i) P_{ref}(k-i), \tag{6}$$

where W_c is the control parameter vector. The output of the system identification p_{in} consists of two parts:

$$\overline{p}_{in}(k) = Y_1(k) + Y_2(k), \tag{7}$$

where the first part Y_1 has the feedforward term with P_{ref} as the input and the feedback term:

$$Y_1(k) = \sum_{j=0}^{N_1} W_{id}^{(11)}(j) P_{ref}(k-j) + \sum_{i=0}^{M_1} W_{id}^{(12)}(l) \overline{P}_{in}(k-l-1) \tag{8}$$

and the second part has the feedforward with the controller output as its input:

$$Y_2(k) = \sum_{j=0}^{N_2} W_{id}^{(21)}(j) V_c(k-j), \tag{9}$$

where W_{id} is system identification parameter vector. They are initialized to a small random value in the beginning. In order to accelerate control convergence speed, [5-7] the signals coming into controller and going out from controller to system identification are normalized to a value between -1 and 1 (the normalizations are signified by *N* in Fig. 2). The absolute value of each sample is compared with a maximum value, if the absolute value of a sample is greater than maximum value, then the maximum value is updated with this new maximum value. If any sample is less than maximum value, it will be normalized by dividing by the maximum value so that the value of any

sample will be between -l and 1. The kth system identification error, $E_{id}(k)$, is defined as

$$E_{id}(k) = \frac{1}{2}(P_{in}(k) - \bar{p}_{in}(k))^2 \tag{10}$$

and is used to update the system identification weights by minimizing the error. The equations for updating the system identification weights are given by

$$W_{id}^{(11)}(k+1) = W_{id}^{(11)}(k) - \eta_s \frac{\partial E_{id}(k)}{\partial W_{id}^{(11)}(k)},$$

$$W_{id}^{(12)}(k+1) = W_{id}^{(12)}(k) - \eta_s \frac{\partial E_{id}(k)}{\partial W_{id}^{(12)}(k)}, \tag{11}$$

$$W_{id}^{(21)}(k+1) = W_{id}^{(21)}(k) - \eta_s \frac{\partial E_{id}(k)}{\partial W_{id}^{(21)}(k)},$$

The explicit expressions for the last term in the above equations can be derived as the following:

$$\frac{\partial E_{id}(k)}{\partial W_{id}^{(11)}(j)} = -(P_{in} - \tilde{P}_{in})P_{ref}(k-j),$$

$$\frac{\partial E_{id}(k)}{\partial W_{id}^{(12)}(l)} = -(P_{in} - \tilde{P}_{in})Y_1(k-l-1), \tag{12}$$

$$\frac{\partial E_{id}(k)}{\partial W_{id}^{(21)}(j)} = -(P_{in} - \tilde{P}_{in})V_c(k-j),$$

respectively. Similar to updating system identification weights, the kth control error, $E_c(k)$, which is used to update the weights of the controller, is defined as

$$E_c(k) = \frac{1}{2}\tilde{P}_{in}^2 \tag{13}$$

and the equations for updating the weights of the controller are

$$W_c(k+1) = W_c(k) - \eta_c \frac{\partial E_c(k)}{\partial W_c(k)}, \tag{14}$$

The explicit expression for the last term can be written as

$$\frac{\partial E_c(k)}{\partial W_c(i)} = \overline{P}_{in} \sum_{j=0}^{N_2} W_{id}^{(21)}(j) P_{ref}(k-i-j), \tag{15}$$

The adaptive controller with on-line system identification was developed in this section. The performance of the controller will be discussed in the next section.

III RESULTS

The experimental simulations for the uncontrolled and controlled plate-cavity system are analyzed using acoustic harmonic excitation. The external sound source location x_o is 2 m directly above the center of the plate, and the transverse displacement of the plate is calculated at its center. The internal pressure is calculated at the bottom center of the cavity. Relevant PZT parameters are thickness $h_{pzt} = 0.25$ mm, strength constant $d_{31} = 2 \times 10^{-10}$ m/V, and dimensions 0.02 m x 0.02 m. The PZT's are assumed to be bonded to the top and bottom of the plate center symmetrically. The Young's modulus and the Poisson ratio for the PZT's are assumed to be identical to those of the plate.

Figure 3(a) shows the frequency spectra of the uncontrolled plate transverse displacement. The three peaks are due to the plate modes ij = 11, 13, 33 and are located at 41, 180, and 332 Hz, respectively. Figure 3(b) shows the frequency spectra of the uncontrolled internal cavity pressure.

Figure 3a

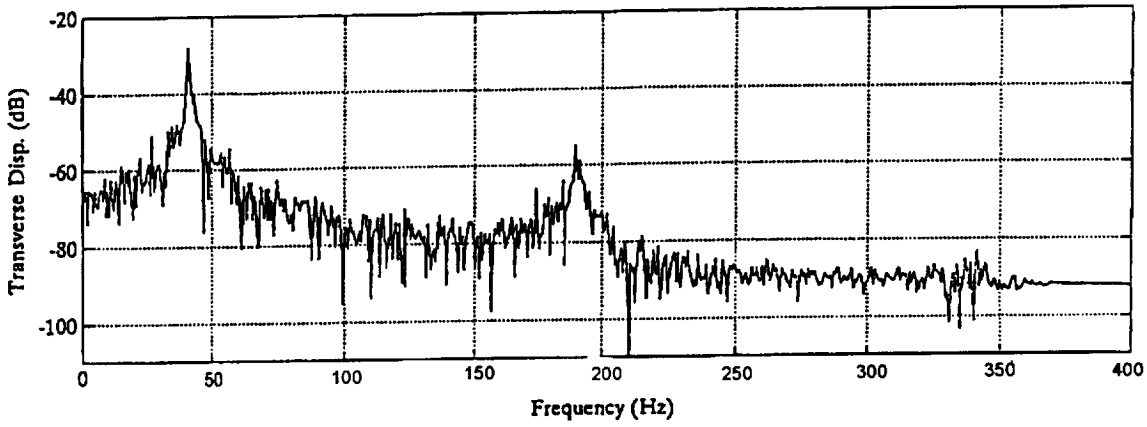

Figure 3b

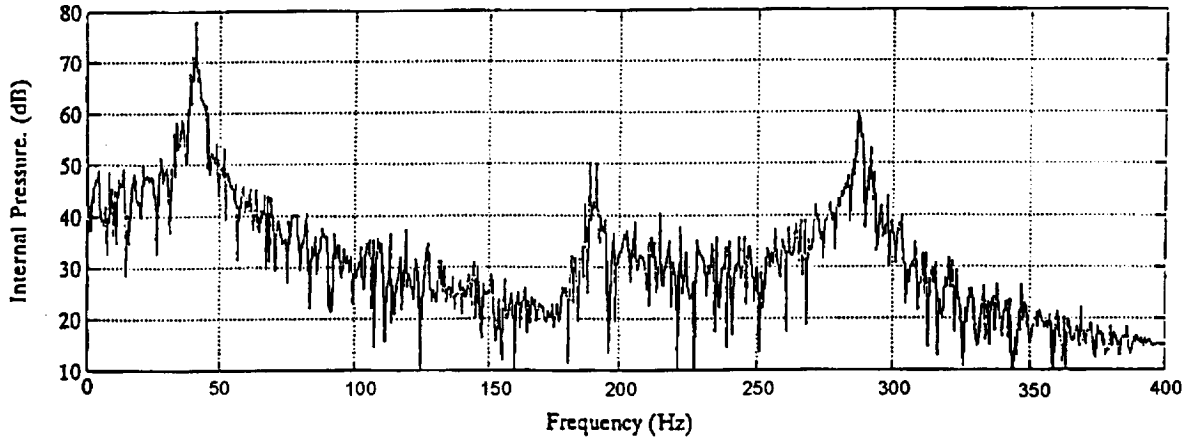

Fig. 3.(a) Frequency response of the uncontrolled displacement at the plate center
(b) Frequency response of the uncontrolled pressure at the cavity top just below the plate.

The pressure peaks corresponding to the plate modes and the additional strong acoustic cavity resonance at 278 Hz are seen in the figure. This cavity resonant mode is not observable through the plate displacement calculation in Fig. 3(a). These figures are obtained for a random acoustic excitation.

The time varying plate-cavity system is used to examine the control performance of the adaptive control for two cases. First, keeping the cavity empty the external disturbance frequency is swept with 1 Hz/s from below to above a resonant frequency of the plate-cavity system.

Figure 4(a) represents the time trace of the uncontrolled internal cavity pressure for the frequency sweep from 31 to 51 Hz in 20 s. The large pressure fluctuation at around 8.5 s is due to the plate mode ij = 11 at 41 Hz. The system identification and the control are simultaneously performed in this algorithm to minimize the cavity pressure. The time trace of the corresponding

Figure 4a

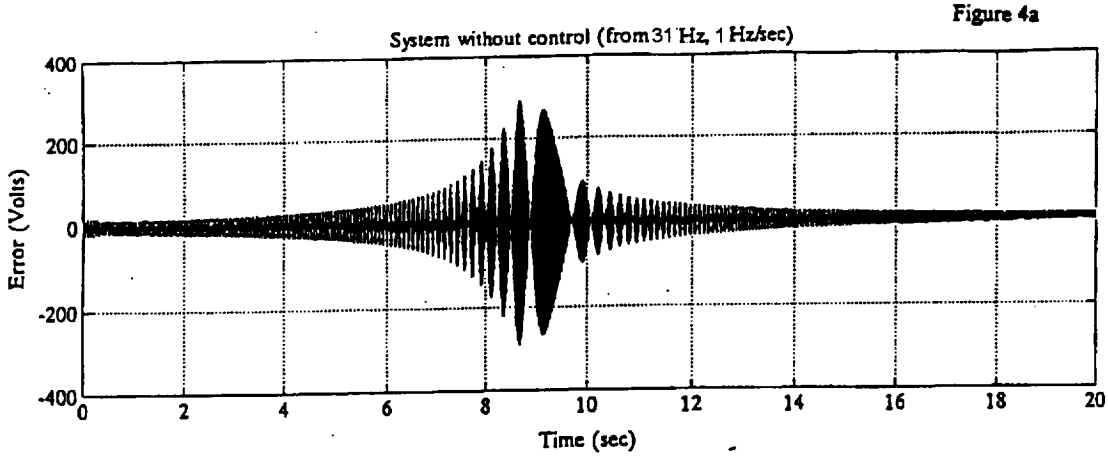

controlled internal cavity pressure in Fig. 4(b) shows an excellent frequency tracking capability with reduction of transmitted sound pressure by 40 dB. Figure 4(c) shows the time history of the system identification error calculated by using Eq. (10). In this run the following parameters are used: $N_c = 10, N_1 = 10, M_1 = 0, N_2 = 10, \eta_c = 0.005$.

Figure 4b

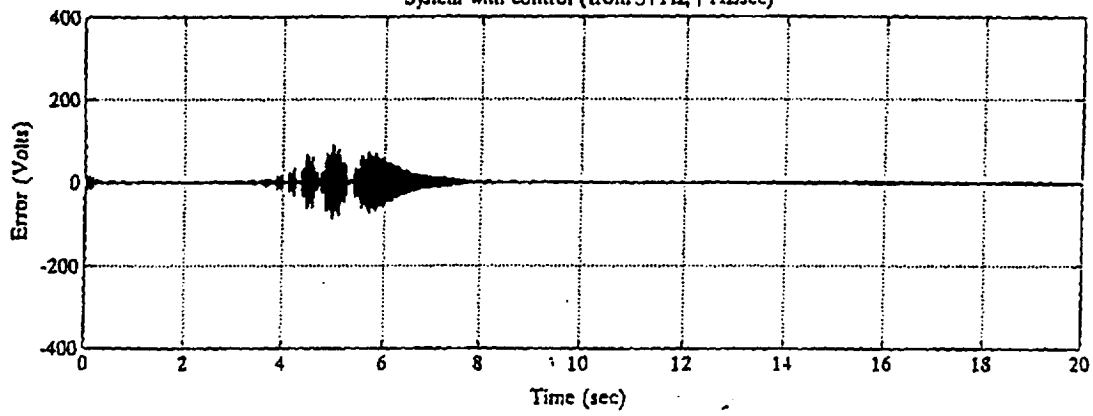

Figure 4c

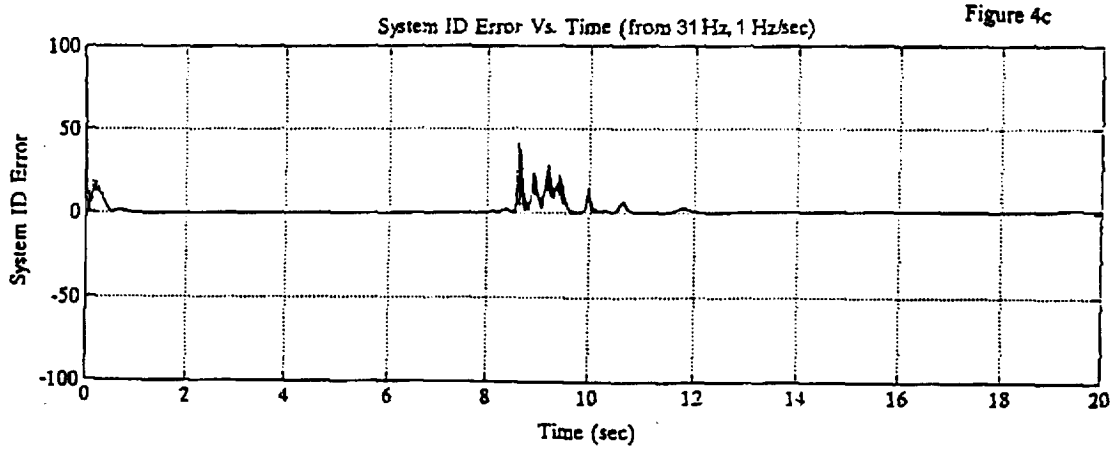

Figure 5a

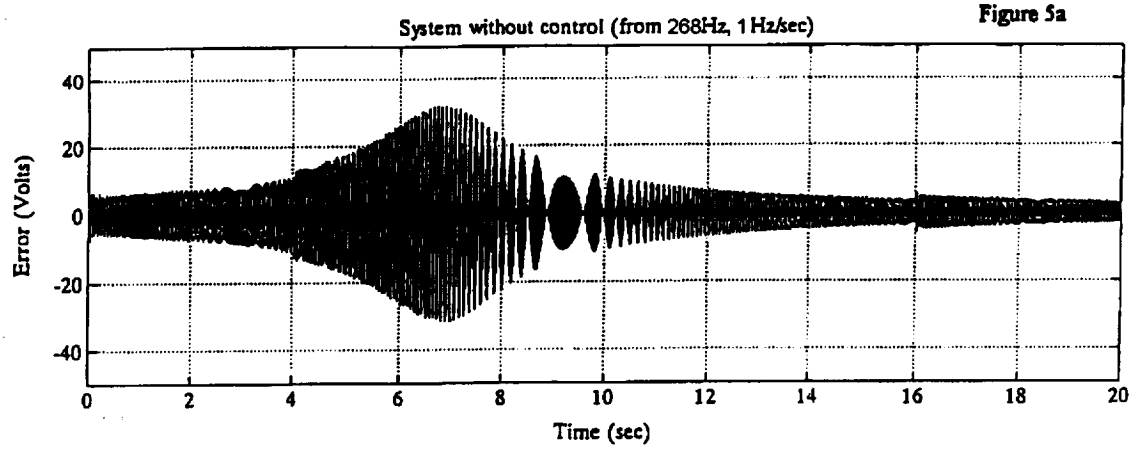

Figure 5b

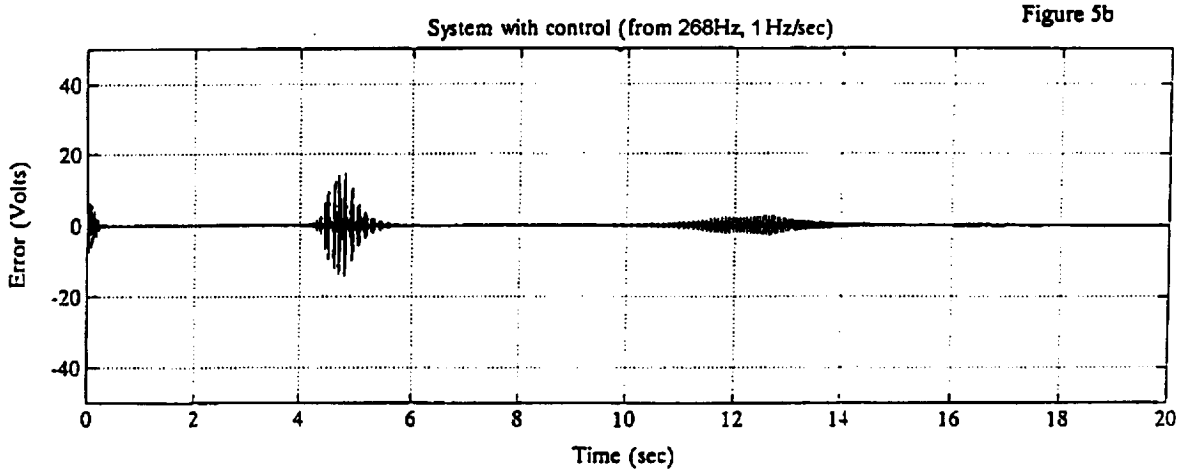

Figure 5c

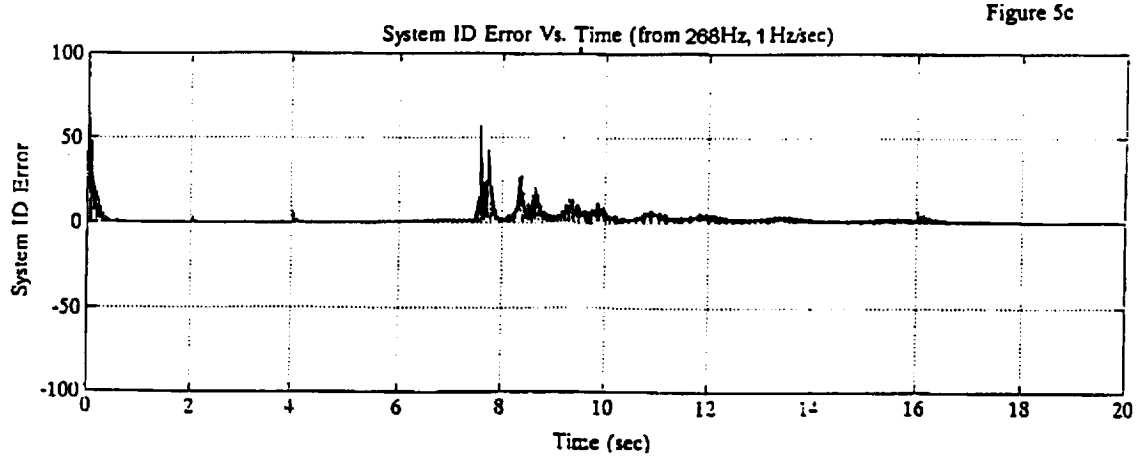

Figure 5(a) represents the time trace of the uncontrolled internal cavity pressure for the frequency sweep from 268 to 288 Hz in 20 s. The large pressure fluctuation at around 7.5 s is due to the cavity acoustic resonance at 278 Hz. The time trace of the corresponding controlled internal cavity pressure in Fig. 5(b) again shows an excellent frequency capability with reduction of transmitted sound pressure by 40 dB. Figure 5(c) displays the similar time history of the system identification error as in Fig. 4(c). The constants η_s and η_c are reduced to 0.0025 in this case.

For the second case, the cavity water level is raised with respect to 3/20 of its full value in 60 s while the external sound excitation is fixed at 287 Hz. Correspondingly, the cavity resonant frequency is increased from 278 to 328 Hz in 60 s. The resonant frequency passes the external sound excitation frequency at around 13 s which is displayed as the large uncontrolled cavity pressure fluctuation in Fig. 6(a). Figure 6(b) shows the case that the controller and on-line system identification are turned on.

Figure 6a

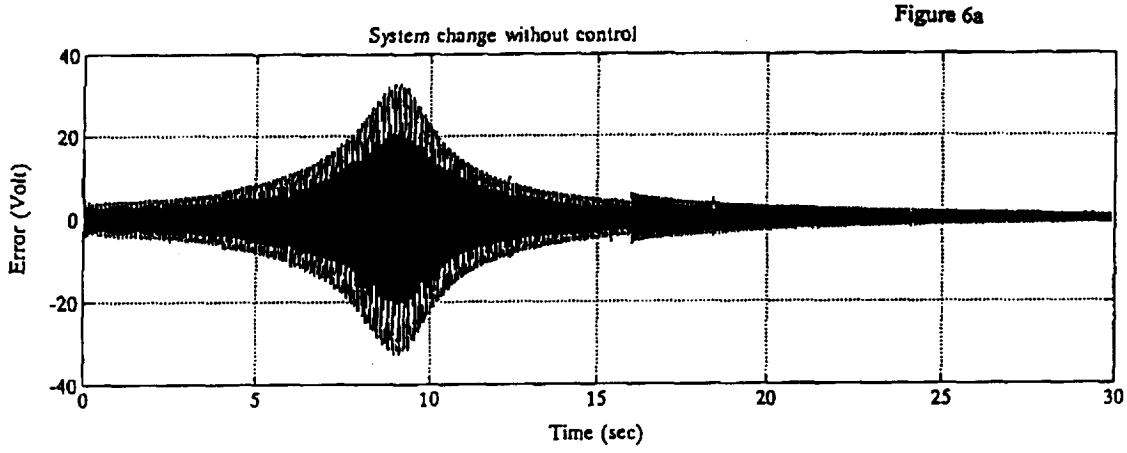

Figure 6b

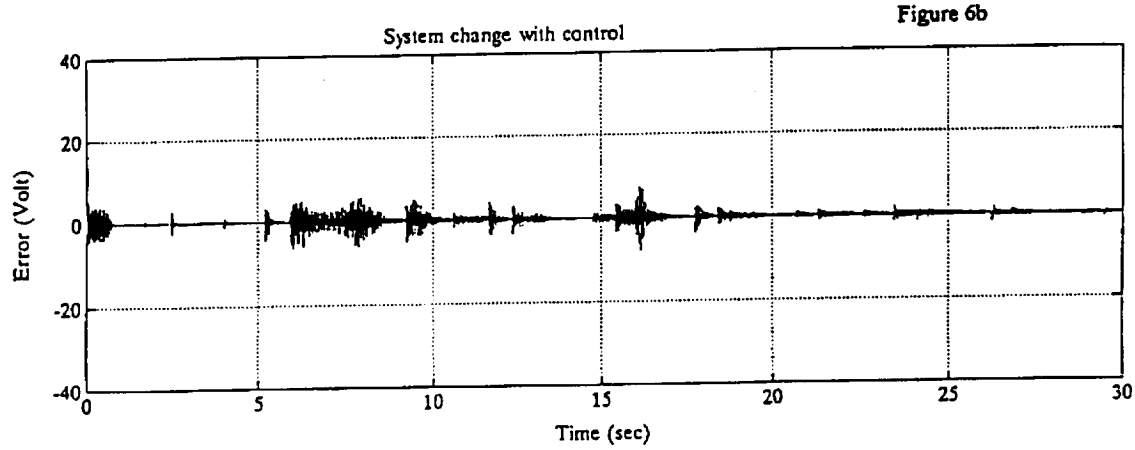

Figure 6c

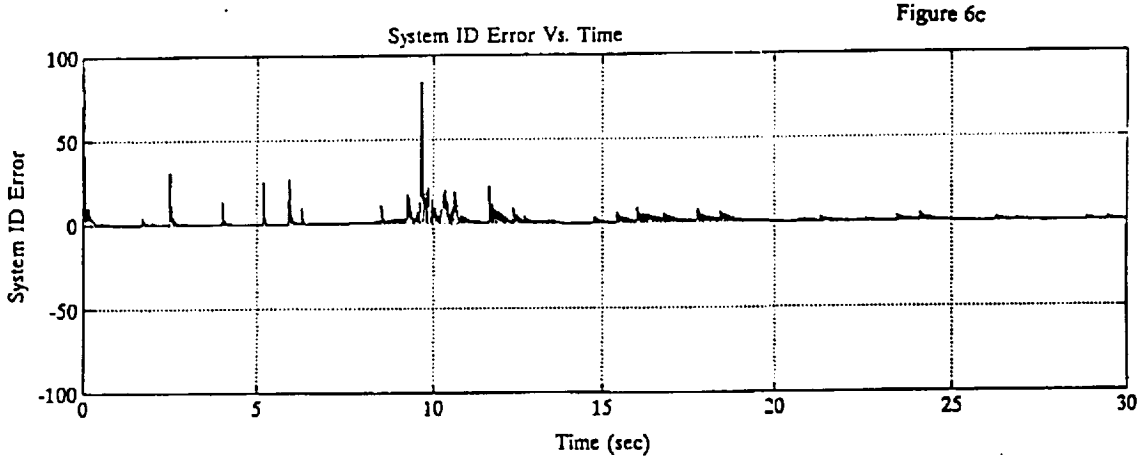

The change in cavity resonant mode is properly identified shown in Fig. 6(c) and the excellent suppression of the cavity resonant pressure of 40 dB is demonstrated in Fig. 6(b). The parameters used for this: $N_c = 10$, $N_1 = 10$, $M_1 = 10$, $N_2 = 10$, $\eta_s = 0.002$, and $\eta_c = 0.002$.

IV CONCLUSION

An adaptive control algorithm with on-line system identification capability has been developed and demonstrated its control capability using the time varying plate-cavity system. One of the great advantages of this algorithm is that an additional system identification mechanism such as an additional uncorrelated random signal generator as the source of system identification is not required. For a given externally located harmonic sound excitation, the system identification and

the control are simultaneously executed to minimize the transmitted sound in the cavity. The control performance of the algorithm is examined for two cases. For the first case, the external disturbance frequency is swept with 1 Hz/s from below to above a resonance frequency of the plate-cavity system. The simulation shows an excellent frequency tracking capability with cavity internal sound suppression of 40 dB. For the second case, the cavity water level is raised to 3/20 of its full value in 60 s while the external sound excitation is fixed with a frequency. The algorithm shows 40 dB transmitted noise suppression without compromising the system identification tracking capability.

ACKNOWLEDGMENTS

This work was supported in part by NASA Langley Research Center, Grant No. NAG1-1697, and the program monitor was Dr. R.J. Silcox.

1. L.J. Eriksson and M.C. Allie, "Use of random noise for on-line transducer modeling in an adaptive active attenuation system," J. Acoust. Soc. Am. 85, 797-802 (1989).

2. S. Koshigoe, J.W. Murdock, "Unified analysis of both active and passive damping for a plate with piezoelectric transducers," J. Acoust. Soc. Am. 93, 346 (1993).

3. S. Koshigoe, A. Teagle, and A. Gordon, "Time domain study of active control of sound transmission due to acoustic pulse excitation," J. Acoust. Soc. Am. 97, 313-323 (1995).

4. S. Koshigoe, J.T. Gillis, and E.T. Falangas, "New approach for active control of sound transmission through an elastic plate backed by a rectangular cavity," J. Acoust. Soc. Am. 94, 900 (1993).

5. Ya. Z. Tsypkin, *Foundations of the Theory of Learning Systems* (Academic, New York, 1973).

6. S. Kaczmarz, "Angenaeherte Auflosung von Systemen Linearen Gleichungen," Bull. Int. Acad. Polon. Sci. Lett. Math. Nat. A (1937).

7. J.I. Nagumo and A. Noda, "A learning method for system identification," IEEE Trans. Automat. Control AC-12, 282-287 (1967).

8. C. Bao, P. Sas, and H. van Brussel, "Comparison of two on-line identification algorithms for active noise control," Proc. of 2nd Conf. on Recent Advances in Active Control of Sound and Vibration, VA, April 1993, pp. 38-54.

9. S.D. Sommerfelt, "Multichannel adaptive control of structural vibration," Noise Control Eng. J. 37(2), 77-89 (1991).